Published in final edited form as:
Nat Cell Biol. 2016 October ; 18(10): 1054–1064. doi:10.1038/ncb3406.

Self-repair promotes microtubule rescue

Charlotte Aumeier[#1,+], **Laura Schaedel**[#1,+], **Jérémie Gaillard**[1], **Karin John**[2], **Laurent Blanchoin**[1,3,*], and **Manuel Théry**[1,3,*]

[1]CytoMorpho Lab, Biosciences & Biotechnology Institute of Grenoble, UMR5168, CEA/INRA/CNRS/Université Grenoble-Alpes, Grenoble, France

[2]Laboratoire Interdisciplinaire de Physique, CNRS / Université Grenoble-Alpes, Saint-Martin-d'Hères, France

[3]CytoMorpho Lab, Hopital Saint Louis, Institut Universitaire d'Hematologie, UMRS1160, INSERM/Université Paris Diderot, Paris, France

[#] These authors contributed equally to this work.

Summary

The dynamic instability of microtubules is characterised by slow growth phases stochastically interrupted by rapid depolymerisations called catastrophes. Rescue events can arrest the depolymerisation and restore microtubule elongation. However the origin of these rescue events remain unexplained. Here we show that microtubule lattice self-repair, in structurally damaged sites, is responsible for the rescue of microtubule growth. Tubulin photo-conversion in cells revealed that free tubulin dimers can incorporate along the shafts of microtubules, especially in regions where microtubules cross each other, form bundles or become bent due to mechanical constraints. These incorporation sites appeared to act as effective rescue sites ensuring microtubule rejuvenation. By securing damaged microtubule growth, the self-repair process supports a mechanosensitive growth by specifically promoting microtubule assembly in regions where they are subjected to physical constraints.

Introduction

Oriented growth of the microtubule network is a key process in the establishment of cell polarity1. The asymmetry of microtubule-network organisation exists in various forms and usually involves differences in the protection of microtubules against depolymerisation. Examples include the selective stabilisation and orientation of microtubules during neuronal axon determination2–4; the selective stabilisation of microtubules toward the leading edge

[*] Correspondence should be addressed to LB (laurent.blanchoin@cea.fr) and MT (manuel.thery@cea.fr).
[+]co-first authors

Authors contribution
CA performed experiments in cells. LS and JG performed the experiments in vitro. LB and MT directed the work. CA, LS, KJ, LB and MT analysed the data. MT wrote the paper.

Competing financial interests.
The authors have no competing financial interests.

Europe PMC Funders Author Manuscripts

of migrating cells5–7 or the basal pole of epithelial cells8; the selective bundling of microtubules toward the immune synapse9; and the stabilisation of a specific subset of microtubules for spindle assembly and orientation10,11. Most attention has been paid to the role of components such as Par312, mDia/APC13, GSK314, IQGAP15 or Lis116 that promote microtubule capture and stabilisation in specific subcellular regions containing defined actin-network compositions. In particular, at the leading edge of migrating cells, microtubules appear to be protected from disassembly that could potentially be induced by the physical barrier of the plasma membrane17. The rescuing of microtubules from depolymerisation is frequent in such regions where actin retrograde flow is active18,5,6,19, and thus the rescue events could actively contribute to local differences in microtubule-network growth. However, the mechanisms controlling the occurrence and modulation of those rescue events are still poorly understood20.

The frequency of rescue events increases with the concentration of free tubulin21 and in presence of MAP2, CLIP170 or CLASP22–24. Their locations appear to be correlated with the presence of short GTP-tubulin stretches along the microtubule shaft25,26, but the origin of these stretches is still debated20. Recently, in response to bending arising from mechanical perturbations, microtubules have been shown to be capable of self-repair by the incorporation of free tubulin dimers into fractured points of the microtubule lattice27. This process of self-repair generates stretches of new tubulin dimers along microtubule length reminiscent of those GTP-tubulin stretches described previously25. It is therefore tempting to hypothesize that microtubule repair sites act as rescue sites. However, microtubule self-repair has not yet been described in vivo and the mechanism by which it could promote microtubule rescue, alone28 or with the help of MAPs23,24,29,30, still need to be investigated.

Results

Microtubule repair in living cells

The investigation of microtubule repair requires free tubulin dimers to be distinguishable from polymerised dimers so that their incorporation into the microtubule lattice can be detected. Local photo-conversion of mEOS2-tubulin was used to convert some of the green-fluorescent dimers into red-fluorescent dimers (Fig. 1a; where red fluorescence is depicted as magenta). These red-fluorescent dimers rapidly diffused through the cell cytoplasm and became available for incorporation throughout the entire cell. A few minutes after photo-conversion (Supplementary Video 1), spots of red-fluorescent tubulin could be observed at the growing tips of microtubules, as well as along the shafts of pre-existing microtubules (Fig. 1a-I, Supplementary Video 2). Microtubules often grow along pre-existing ones. Therefore a local patch of red tubulin along a green microtubule shaft may correspond to a growing secondary microtubule rather than a site of red-tubulin incorporation into the green primary microtubule. However, in the former case, fluorescence intensity should increase over time along the original microtubule, concomitantly with the local incorporation of red tubulin at the growing tip. By observing microtubule fluorescence over several minutes before and after the appearance of red patches, we considered that no change in the fluorescence at the site of the initial red-fluorescent patch implied that tubulin was

incorporated into the pre-existing lattice (Fig. 1a-V and V-kymograph). From this analysis, most of the tubulin-incorporation sites were located at microtubule crossovers (Fig. 1a-II, a-III) or in highly curved regions (Fig. 1a-IV). Interestingly, microtubule crossovers are known to recruit katanin31,32, which has a strong affinity for sites of damaged lattice33,34, suggesting that the incorporation sites were genuine repair sites. Incorporation sites were also frequently observed along microtubules forming bundles (Fig. 1a-I, 1b), although in those cases, it was hard to confirm that the sites did not correspond to growing plus-ends.

Microtubule rescue at repaired sites in living cells

When following microtubule dynamics next to the repair sites, we found that with a microtubule undergoing catastrophe, depolymerisation was arrested and regrowth was initiated precisely at the location of the repair site (Fig. 2a, Supplementary Video 3). Unfortunately, it was experimentally challenging to repeat these observations in regions where the network was sufficiently sparse to follow single microtubules, and in regions where rescues were likely to occur18. Alternatively, we decided to record the locations of microtubule rescue events near the cell margin where microtubules show a high rescue frequency26 (Fig. 2b,c,d) and compare the locations of rescue sites with those of incorporation sites (Fig. 2e). We found that most rescues occurred close to the microtubule tip (Fig. 2d) at microtubule crossovers (60%) (Supplementary Video 4) or at curved regions (30%) (Fig. 2e). Strikingly, the relative frequencies of microtubule rescues with respect to three different types of microtubule structure (crossover, curved and straight) precisely matched the relative frequencies of incorporation sites (Fig. 2e).

Microtubule rescue at laser-induced photo-damaged sites

To further validate this correlation at the single-microtubule level, and more directly, to test whether the repair of structural damage in the microtubule lattice was responsible for the rescue events, we selected a method to modulate microtubule damage and repair in space and time. This method used focused laser light, which was above the power required for bleaching but below the severing threshold, and can induce local damage and promote further self-repair of microtubules27,35 (Supplementary Fig. 1a). The method both ensured the genuine occurrence of lattice damage on targeted sites and allowed the monitoring of potential consequential changes in microtubule dynamics at the same sites. We first confirmed that laser-induced photo-damage could trigger lattice self-repair by photo-converting mEOS2 tubulin and then focusing the laser on a straight and central section of the microtubule, more than two microns away from the microtubule end, where rescues were unlikely (Supplementary Fig. 1b). Photo-converted free tubulin was rapidly incorporated at the photo-damaged sites, confirming the effectiveness of the laser to induce microtubule damage and repair (Fig. 3a). Furthermore, we observed rescue events at the incorporation sites that were subsequent to microtubule depolymerisation events (Fig. 3b). This behaviour was further quantified by recording the location of the rescue sites with respect to the damaged site (Fig. 3c-e Supplementary Video 5, 6). Photo-damaged microtubules rescued more frequently (75%, 41/55, Fig. 3g) within a timeframe of 4 min than non-photo-damaged microtubules (39%, 24/62). The increased frequency is due to additional rescue events occuring next to the photo-damaged site, regardless its position along the microtubule (Fig. 3d-e, Supplementary Videos 5 and 6). Noteworthy, repair by incorporation of new dimers

was tightly focused and did not occur over the entire length of the targeted region, but rescues systematically occurred at the exact position of the repair site either on the right or on the left of the targeted region (Fig. 3b). These results clearly showed that microtubule damage and repair provided the microtubule with protection from depolymerisation. Interestingly, some observations suggested that the protective effect did not last indefinitely (Fig. 3f). More quantitative experiments of longer duration further revealed that protection was quite effective within a two-minute period after photo-damage. However, protection was progressively less effective from 2 to 8 minutes after photo-damage (Fig. 3g). This effect of time showed that the microtubule repair and rescue events were not due to permanent structural changes and suggested that additional biochemical regulation was involved at longer time scale.

Microtubule self-repair and rescue in vitro

At the repair site, newly incorporated dimers were certainly associated with GTP tubulin, as is the case for dimer assembly at the growing end of the microtubule. Hence the subsequent rescue event could have depended on intrinsic structural factors, such as the specific conformation of GTP-tubulin dimers36, and extrinsic factors, such as the numerous proteins preferentially interacting with GTP-tubulin dimers23,24,29,30. To elucidate the mechanism of microtubule rescue after damage and repair events, and to identify the minimal conditions sufficient to support the mechanism, we performed *in vitro* experiments based on purified tubulin dimers that self-assembled to form microtubules on glass slides. This setup provided more defined conditions than in vivo and could be used to challenge the role of MAPs during rescue at incorporation sites.

We first investigated the rescue events in networks of dynamic microtubules. They appeared preferentially localized at crossing sites (Fig. 4a,b, Supplementary Video 8, see Methods) confirming our observations in vivo (Fig. 2c,e). To test whether these sites corresponded to self-repair events based on free tubulin incorporation, we screened long microtubules, assembled from red tubulin and stabilized with a GMPCPP cap, in a medium containing free green tubulin dimers. Self-repair indeed occurred at crossing sites (Fig. 4c). Half of the 300 crossing sites (from 3 independent experiments) displayed incorporation of free tubulin in the seven minutes following free tubulin exchange.

To further quantify the repair and rescue events in single dynamic microtubule in controlled environment, microtubules were assembled in a microfluidic device. Short microtubule fragments were adsorbed onto micropatterned lines and used as seeds to induce microtubule polymerization. Micropatterned lines were surrounded with PEG to minimize microtubule interactions with the glass-slide surface37. The micropatterned glass coverslips were mounted on a microfluidic circuit to modulate the addition and removal of soluble components without moving the microtubules under observation27 (Fig. 4d). Laser light was used to generate photo-damage on dynamic microtubules. As expected from our previous work27, photo-damaged microtubules self-repaired by incorporating free tubulin in the damaged site (Supplementary Figure 2). In the absence of photo-damage, rescue events were occasional (in 18 out of 78 microtubules) and randomly dispersed along the microtubule (Fig. 4e,f). By contrast, most photo-damaged microtubules underwent depolymerisation that

was subsequently rescued (50 out of 76 microtubules, Fig. 4e,f, Supplementary Figure 3, Supplementary Video 7). These rescue events were precisely located at the sites of damage (Fig. 4e) where self-repair occurred (Fig. 4g) showing that damage/repair sites could protect microtubules from depolymerisation independently of the presence of MAPs or any other cellular compound.

Incorporation and hydrolysis of free tubulin

We then tested whether repair was actually required for rescue or whether damage in the lattice was sufficient to block microtubule depolymerisation. Microtubules were photo-damaged in the absence of free tubulin to prevent lattice self-repair. We controlled that laser power and frequency were appropriate and did not induce microtubule breakage or lattice cauterization (Supplementary Figure 4). Elongated microtubules were capped with non-hydrolysable GMPCPP tubulin to protect the ends from initiating depolymerisation that would otherwise occur in the absence of free tubulin (Fig. 5a). After a microtubule was photo-damaged, the laser power was increased to sever the cap from the microtubule and trigger microtubule depolymerisation (Methods). Under these conditions, no rescue events, pauses or arrests in depolymerisation were observed at the damaged and non-repaired sites (Fig. 5a). This showed that lattice self-repair by the incorporation of free-tubulin dimers was essential to protect the microtubule from depolymerisation. Moreover, this dependency on free tubulin could account for the observations that rescue frequency also depends on the concentration of free tubulin21,24. Interestingly, it appeared that the protective capacity provided by the repair site, in the presence of free tubulin, was limited by time, similar to what was observed in vivo. Rescue events were frequent within 3 minutes after the damage/repair event (73%, 38/52), but less frequent from 3 to 20 minutes after the damage/repair event (30%, 14/47) (Fig. 5b). Nucleotide hydrolysis following tubulin polymerization at the microtubule tip effecting the conformation and stability of lattice structure38, we therefore tested whether hydrolysis was involved in rescue regulation. We compared the rescuing frequency at repair sites depending on the insertion of free tubulin dimers in the presence of control (GTP) and non-hydrolysable (GMPCPP) nucleotide 5 to 10 minutes after damaging microtubules with the laser (Fig. 5b). As tubulin bound to GMPCPP formed numerous seeds, the rescue effect had to be tested in the presence of sub-critical concentration of free tubulin dimers to prevent the growth of too many additional microtubules next to our observation region. The pauses at the laser-damage site, following cap removal and microtubule depolymerisation, were twice more frequent when microtubules were repaired with tubulin dimers bound to GMPCPP (Fig. 5c), confirming that nucleotide hydrolysis was limiting the rescue lifetime.

Recruitment of MAPs with affinity for GTP-tubulin

At the microtubule growing tip, newly incorporated tubulin dimers together with specific proteins that have high affinity for GTP-bound tubulin form a cap that protects microtubules from depolymerisation 39. These proteins could then be recruited on repair sites, which are also made of GTP-tubulin, and form some cap-like structures that could act as rescue factors23,24,29,30. To test this hypothesis, we grew red-fluorescent microtubules and followed microtubule repair after laser-induced damages, in the presence of red-fluorescent tubulin and a Alexa-488-tagged-end-binding protein 3 (EB3). We found that lattice

damaging, which we could visualize by the reduction of fluorescent tubulin along the lattice, was associated to a specific recruitment of EB3 at the repair site (Fig. 5d). Interestingly, this recruitment was firmly dependent on the incorporation of free tubulin at the damaged site since it could not be detected in the absence of free tubulin (Supplementary Figure 5). Therefore the self-repair process induced GTP-island resembling cap structures along the microtubule lattice that are able to recruit proteins with high affinity for GTP-tubulin. Although we could not detect such recruitment in cells following laser-induced damage because of the high background of cytoplasmic EBs, this cap could contribute to the rescue process in vivo23,24,29,30. However, our previous data in vitro showed that the incorporation of free tubulin was necessary (Fig. 5a) and sufficient (Fig. 4b) to promote microtubule rescue. Microtubule repair by free tubulin incorporation conditioned the recruitment of EBs and associated proteins, which may contribute but did not appear required to promote microtubule rescues.

Repeated damages lengthen microtubule protection from depolymerisation

In vitro, single event of microtubule repair had a time-limited effect on microtubule dynamics. We reasoned that in vivo the duration of protection against depolymerisation could be extended in situations when repair events occur frequently, e.g. at the cell margin where microtubules often crossover their neighbours, form bundles and are repeatedly bent by the retrograde flow of actin6. Indeed, repeated photo-damage near the tip of microtubules growing in vitro in the presence of 12 μM of tubulin could prevent catastrophic depolymerisation for more than 20 minutes, whereas, in the absence of damage, depolymerisation frequently occurred within 5 minutes (Fig. 6a,b, Supplementary Fig. 6, Supplementary Video 9). Therefore, damaged microtubules became much longer (Fig. 6c). Remarkably, the targeting of individual microtubules using the same approach in vivo had similar consequences. We focused on peripheral cell parts where microtubules were sparse. To compare the effects of laser-induced damages on microtubules to the non-specific damages the laser may cause to all surrounding components, pulses were simultaneously sent to two distinct sub-cellular regions. In one the laser impacts targeted the microtubules, in the other they were focused next to microtubules (Figure 7a). The evolution of the microtubule network was followed over 10 to 15 minutes during which both regions were subjected to repeated laser pulses (Fig. 7a, Supplementary Video 10). Laser-induced photo damage of every microtubule that approached the cell margin robustly protected those microtubules from depolymerisation and promoted their elongation whereas no net extension of the network was seen when impact were off-target (Fig. 7b, Supplementary Video 10). The damaged microtubules underwent multiple rescue events, continued to grow and eventually aligned parallel to the cell edge (Supplementary Fig. 7, Supplementary Video 10). These effects were quantified by measuring the ratio of fluorescent tubulin before and after the laser-induced damages on the two windows of laser pulses. No net growth was detected when laser impacts were off-target whereas an average of 50% increase was measured when impacts were focused on microtubules (Fig. 7b). Strikingly, cells then tend to move toward this newly defined leading edge (Fig. 7a, Supplementary Fig. 8, Supplementary Videos 10,11). These observations were consistent with the known enhancement of cell motility in response to microtubule overgrowth following down-regulation of microtubule severing enzymes40,41. Therefore damage and self-repair

appeared capable of sustaining microtubule polymerisation in cells and affect higher-order processes such as modulating the polarity of a motile cell.

Discussion

Our results have revealed a mechanical and structural mechanism by which a damaged microtubule can acquire a capacity to prevent its catastrophic depolymerisation through the incorporation of new dimers of tubulin.

Incorporation could be directly visualised thanks to the monitoring of photo-converted tubulin dimers. It occurred not only at microtubule ends but also along the microtubule shaft. It was not randomly distributed along the microtubule length but preferentially located in regions where the lattice is likely to be submitted to geometrical and mechanical constraints such as microtubule crossover, bundle and bending sites (Fig. 8a). Solid friction between adjacent microtubules42 and microtubule bending by guiding motors43 or surrounding networks6 are general source of mechanical stress in the lattice which could promote protofilament peeling and dimer removal. Although our observations of lattice turnover at microtubule crossover in vitro did not involve any additional component than the physical constraints on microtubules27, proteins with specific affinity for these network conformations, such as bundling proteins, may contribute to the lattice turnover via their binding to tubulin dimers44. In return, the appearance of new protofilament ends and the incorporation of new tubulin dimers at damaged sites may promote the local recruitment of specific proteins, such as EB3 in our observations. Katanin for example, which is known to localize at microtubule crossovers32, may be recruited according to its affinity for the damaged lattice and further benefit from the open structure to sever microtubules. Similarly, doublecortin, which recognize plus-ends and bent regions may benefit from lattice damaging and turnover for their targeting45. The high degree of microtubule lattice plasticity revealed by our data opened many interesting perspectives in the regulation of microtubule-associated proteins.

Microtubule lattice plasticity also impacts microtubule dynamics, since the incorporation of new dimers rejuvenates the lattice. Our observation of red tubulin stretches along green microtubule length, which had already been indirectly observed with antibodies directed against the GTP-conformation of tubulin dimers25, signed the implication of external tubulin incorporation for lattice repair, rather than internal lattice remodelling, at damaged sites. As was reported for the GTP-stretch25, we found that the newly incorporated dimers were responsible for microtubule rescue (Fig. 8b). Hence the repair sites appear to act as plus-end-like “mini cap” that can protect the microtubule from depolymerisation and support subsequent elongation. Importantly, our in vitro experiments show that the incorporation of new tubulin dimers in the absence of MAPs is sufficient to rescue microtubule depolymerisation. However, we documented the ability of newly incorporated dimers to recruit EB3. Additional MAPs with high affinity for GTP-tubulin, such as CLASP, could also be recruited and further contribute to the rescue mechanism in cells23,24,29,30. So microtubule rejuvenation by incorporation of new tubulin dimers could synergize with MAPs recruitment to enhance the autonomous rescuing capacities of repair sites.

Europe PMC Funders Author Manuscripts

Europe PMC Funders Author Manuscripts

Finally, the repair and rescue mechanism we described biases the dynamic instability of the microtubule in a direction where the lifespan and maximal length are greater than would have occurred in a stochastic process without damage. What is also notable is that the repair process provides a mechano-sensitive feedback loop that specifically promotes microtubule extension in intracellular regions where network entanglement and physical constraints are higher, and hence supports the directed growth of the microtubule network within the cell.

Methods

Imaging

Microtubules were visualized using an objective-based azimuthal ilas2 TIRF microscope (Nikon Eclipse Ti, modified by Roper Scientific) and an Evolve 512 camera (Photometrics). The cell culture conditions on the microscope stage were controlled with the Chamlide TC incubator (kept at 37°C and 5 % CO2). For in vitro experiments, the microscope stage was kept at 37°C by means of a warm stage controller (LINKAM MC60). Excitation was achieved using lasers with wavelengths of 491 and 561 nm (Optical Insights). Time-lapse recording was performed using Metamorph software (version 7.7.5, Universal Imaging). Movies were processed to improve the signal/noise ratio (subtract background, smooth and PureDenoise functions of ImageJ, version 1.47n5). The Kymographs corresponding to the time-lapse sequences were drawn using ImageJ. Images were taken every 300 ms to 5 s (in vitro) and 3 s to 7 s (microtubule dynamics in vivo) or 10 s to 2 min (cell migration). For in vitro experiments showing incorporation of labelled tubulin in photo-damaged microtubules, 30 successive individual images were overlaid and background subtracted.

Live cell imaging

PtK2 cells stably expressing GFP-tubulin (a kind gift of Dr. F. Perez, Curie Institute, Paris, France) were cultured on glass coverslips for microscopy. The PTK2 cell line (Sigma Aldrich) was transfected with Lipofectamine®2000 (ThermoFisher Scientific) according to protocol with the photo-conversion protein fused to tubulin mEOS2-tubulin (a kind gift from Michael Davidson, Addgene plasmid # 57431). All cell lines were tested monthly for mycoplasma contamination. No cell lines used in this study were found in the database of commonly misidentified cell lines that is maintained by ICLAC and NCBI Biosample . We did not attempt to authenticate them. For long time imaging (10 min, timeframe 4 s) after photo-conversion the stable PtK2 GFP-tubulin cell line was transfected with the mEOS2-tubulin construct to overcome bleaching of the unconverted green signal. Photo-conversion was achieved with a 100 mW/405 nm laser used at 9% power, performing 15 repetitions within a field size varying between 12 μm × 12 μm to 30 μm × 30 μm.

Fixation

Cells expressing mEOS2-tubulin were fixed 2 min after photoconversion. Cells were detergent-extracted with BRB80 + 4 mM EGTA supplemented with 0.2% Triton X-100 at 37 ° for 15 s. Glutaraldehyde and Triton X-100 were added to a final concentration of 0.5% each and cells were fixed for 10 min. Cells were rinsed twice using PBS supplemented with 1% Triton X-100 and incubated twice with 1% NaBH4 in PBS for 7 min. Cell were rinsed in PBS and imaged. 10 cells from 4 independent experiments were analysed.

Laser-induced microtubule photo-damage

Laser-induced microtubule photo-damages were performed using a Laser illuminator iLas2 (Roper Scientific) set up on an inverted microscope (Ti-E, Nikon) with a ×100 Nikon APO TIRF Oil-immersion objective plus an optical lens x1.45. iLas2 is a dual-axis galvanometer-based optical scanner that focuses the laser beam on the sample (diffraction-limited spot size) over the whole field of view of the camera. Laser displacement, exposure time, frequency and repetition rate were controlled using Metamorph software (version 7.7.9.0, Universal Imaging). To damage the microtubules of the GFP-tubulin or mEos2-tubulin cell line, a 200 mW/491nm laser was used at 40% power, performing 300 repetitions within a field size of approximately 1 μm × 1 μm. To analyse the long-term effect of laser induced photo-damage with respect to rescue, microtubules where multiple photo-damaged along the lattice (twice or three times). This increased the lifetime of the microtubule and the damage furthest away from the plus tip was taken into account for the analysis.

We then analyse the effect of locally increased microtubule lifetime due to laser damaged in cells. PtK2 GFP-tubulin cells were imaged over 10 min. We photo-damaged single microtubules within a region of the cell margin for 5 to 7 min. Within the same timeframe we simultaneously applied the same laser energy next to microtubules at a distant cell margin region (Fig S7). The mean fluorescent intensity of GFP-tubulin was measured in both areas before (0 min) and after (10 min) laser impact. After subtraction of the intensity decrease due to photo-bleaching the ratio fluorescent intensity before and after laser-damage was calculated for the site within the cells were microtubule were damaged and the site were laser was applied next to the microtubule. 16 cells were analysed from 4 different experiments.

For in vitro experiments, ATTO-488-labelled microtubules were damaged using a 100 mW / 491 nm laser with a x60 Nikon APO TIRF Oil-immersion objective. To test the effects of frequency (corresponding to the number of points per second) and laser power, GMPCPP capped microtubules were damaged in the absence of free tubulin and the frequency was varied between 1000 s^{-1} and 10000 s^{-1} and the laser power between 3% and 100% of the maximum power (supplementary Fig. 3). The GMPCPP cap was removed using a laser pulse to initiate depolymerisation. At low laser power and frequency, microtubules depolymerized without pausing. At high laser power and low frequency, microtubules were cut at the laser damage site and immediately depolymerized afterwards. At low laser power and high frequency, most microtubules either broke, pausing for a short time before depolymerisation, or paused at the laser damage site. At high laser power and frequency, microtubules mostly paused at the damage site. For all other experiments involving laser damage in vitro, low laser power (4-9%) and frequency (2500 s^{-1}) were chosen.

Tubulin purification and labelling

Tubulin was purified from fresh bovine brain by three cycles of temperature-dependent assembly and disassembly in Brinkley buffer 80 (BRB80 buffer: 80 mM PIPES pH 6.8, 1 mM EGTA and 1 mM MgCl2 plus 1 mM GTP)46. MAP-free neurotubulin was purified by cation-exchange chromatography47 (EMD SO, 650 M, Merck) in 50 mM PIPES, pH 6.8, supplemented with 1 mM MgCl2 and 1 mM EGTA. Purified tubulin was obtained after a

cycle of polymerization and depolymerisation. Fluorescent tubulin (ATTO-488 and ATTO-565-labelled tubulin) and biotinylated tubulin were prepared as previously described48. Microtubules from neurotubulin were polymerised at 37°C for 30 min and layered onto cushions of 0.1 M NaHEPES, pH 8.6, 1 mM MgCl2, 1 mM EGTA, 60% v/v glycerol, we resuspended the pellet in 0.1 M NaHEPES, pH 8.6, 1 mM MgCl2, 1 mM EGTA, 40% glycerol and labelled by adding 1/10 volume 100 mM ATTO-488 NHS ester, we stopped the reaction by adding 2 volumes 160 mM PIPES, 2 mM MgCl2, 2 mM EGTA, 100 mM potassium glutamate and 40% v/v glycerol, and then microtubules were sedimented onto cushions of BRB80 supplemented with 60% glycerol. Microtubules were resuspended in BRB80, and a second cycle of polymerization and depolymerisation was performed before use.

Cover glass micropatterning

The micropatterning technique was adapted from Portran et al37. Cover glasses were cleaned by successive chemical treatments: 30 min in acetone, 15 min in ethanol (96%), rinsing in ultrapure water, 2 h in Hellmanex III (2% in water, Hellmanex), and rinsing in ultrapure water. Cover glasses were dried using nitrogen gas flow and incubated for three days in a solution of tri-ethoxy-silane-PEG (30 kDa, Creative PEGWorks) or a 1:10 mix of tri-ethoxy-silane-PEG-biotin and tri-ethoxy-silane-PEG at 1 mg ml^{-1} in ethanol 96% and 0.02% HCl, with gentle agitation at room temperature. Cover glasses were then successively washed in ethanol and ultrapure water, dried with nitrogen gas, and stored at 4°C. Passivated cover glasses were placed into contact with a photomask (Toppan) with a custom-made vacuum-compatible holder and exposed to deep ultraviolet light (7 mW cm^{-2} at 184 nm, Jelight) for 3 min. Deep ultraviolet exposure through the transparent micropatterns on the photomask created oxidized micropatterned areas on the PEG coated cover glasses.

Microfluidic circuit fabrication and flow control

The microfluidic device was fabricated in PDMS (Sylgard 184, Dow Corning) using standard photolithography and soft lithography. The master mould was fabricated by patterning 50-µm-thick negative photoresist (SU8 3050, Microchem) by photolithography using a custom made photolithographic mask (La Composite, France). A positive replica was fabricated by replica moulding PDMS against the master. Before moulding, the master mould was vapour silanized (trichloro(1H,1H,2H,2H-perfluorooctyl)silane, Sigma) for easier lift-off. Two inlet/outlet ports were made in the PDMS device using 0.5 mm soft substrate punches (UniCore 0.5, Ted Pella). Connectors to support the tubing were made out of PDMS cubes (0.5 cm side length) with a 1.2 mm diameter through-hole. The connectors were bonded to the chip ports using still liquid PDMS as glue, which was used to coat the interface between the chip and the connectors, and was then rapidly cured on a hotplate at 120°C. Teflon tubing (Tefzel, inner diameter: 0.03”, outer diameter: 1/16”, Upchurch Scientific) was inserted into the port serving as an outlet. Tubing with 0.01” inner and 1/16” outer diameter was used to connect the inlet, via a three-way valve (Omnifit Labware) that could be opened and closed manually, to a computer-controlled microfluidic pump (MFCS-4C, Fluigent). Flow inside the chip was controlled using the MFCS-Flex control software (Fluigent).

Microtubule growth on micropatterns

Microtubule seeds were prepared at 10 μM tubulin concentration (20% ATTO-565 or ATTO-488-labelled tubulin and 80% biotinylated tubulin) in BRB80 supplemented with 0.5 mM GMPCPP at 37°C for 1 h. The seeds were incubated with 1 μM Taxotere (Sigma) at room temperature for 30 min and were then sedimented by centrifugation at 30°C and resuspended in BRB80 supplemented with 0.5 mM GMPCPP and 1 μM Taxotere. Seeds were stored in liquid nitrogen and quickly warmed to 37°C before use.

For experiments involving exchange of the solution after microtubule growth, the PDMS chip was placed on a micropatterned cover glass and fixed on the microscope stage. The chip was perfused with neutravidin (25 μg ml-1 in BRB80; Pierce) and washed with BRB80. Microtubule seeds were flowed into the chamber at high flow rates perpendicularly to the micropatterned lines to ensure proper orientation of the seeds. Non-attached seeds were washed out immediately using BRB80 supplemented with 1% BSA. Seeds were elongated with a mix containing 12 - 20 μM of tubulin (20% labelled) in BRB80 supplemented with 50 mM NaCl, 25 mM NaPi, 1 mM GTP, an oxygen scavenger cocktail (20 mM DTT, 1.2 mg ml-1 glucose, 8 μg ml-1 catalase and 40 μg ml-1 glucose oxidase), 0.1% BSA and 0.025% methyl cellulose (1500 cp, Sigma). For experiments showing tubulin incorporation after photo damage, a solution of 100% labelled tubulin was perfused before applying the laser damage. GMPCPP caps were grown by supplementing the before mentioned buffer with 0.5 mM GMPCPP (Jena Bioscience) and using 10 μM tubulin (100% labelled). Only microtubules growing in the direction of flow were analysed. For depolymerization experiments, the same mix as for microtubule elongation was used, without adding free tubulin to it.

For rescue experiments after photo damage, a flow cell chamber with an approximate volume of 40 μl was constructed with double-sided tape (70 μm height) between a micropatterned cover glass and a passivated glass slide. The chamber was perfused with 25 μg ml-1 neutravidin (Pierce) and washed with 300 μl of BRB80. Microtubule seeds were perfused and non-attached seeds were removed by washing with 300 μl BRB80 supplemented with 1% BSA. Seeds were elongated with a mix containing 12 μM of tubulin (20% labelled and 80% unlabelled tubulin) as described above. Only microtubule plus ends were considered for analysis.

For repair and rescue experiments after photo damage, microtubules were grown with red fluorescent tubulin (20% labelled with ATTO-565 and 80% unlabelled, 20 μM) from micropatterns. Microtubules were then protected from depolymerization by growing a cap at microtubule ends with 0.5 mM GMPCPP and 10 μM tubulin. The solution was then replaced by 20 μM ATTO-488-labelled tubulin (100% labelled) and microtubules were photo damaged. After waiting approx. 2 min, the solution was replaced by red fluorescent tubulin (18 μM, 20% labelled) and microtubule dynamics were initiated by removing the GMPCPP cap with a laser pulse at high intensity.

For microtubule crossing and rescue experiments, microtubules were grown from seeds randomly attached via neutravidin to cover glasses passivated with a mix of tri-ethoxy-

silane-PEG-biotin and tri-ethoxy-silane-PEG. Microtubule dynamics were imaged for 30 min.

For repair and pause experiments in presence of GMPCPP- and GTP-tubulin, microtubules were grown with red fluorescent tubulin at 20 μM (20% labelled). Microtubules were then capped as described above with GMPCPP-tubulin. Laser damage was initiated either in the presence of 10 μM green fluorescent GMPCPP-tubulin or 15 μM green fluorescent GTP-tubulin (100% labelled). After waiting approx. 2 min, the solution was replaced by 10 μM red fluorescent GTP-tubulin (20% labelled) and depolymerization was initiated by cutting the GMPCPP cap with a laser pulse at high intensity after a delay of 200-400 s.

Microtubule crossing experiment

A flow cell chamber with an approximate volume of 40 μl, two entry and two exits sites was constructed with double-sided tape (70 μm height) between a glass coverslips functionalized with SiPEG-Biotin49 and a passivated glass slide (SiPEG 30kDa). The chamber was perfused with 25 μg ml-1 neutravidin (Pierce) for 1 min and washed with 300 μl of BRB80. Microtubule were polymerized for 30 min from microtubule seeds (0.5 μM) in a tub with an elongation mix containing BRB80, 1 mM GTP and 20 μM of tubulin (10% ATTO-565-labelled and 90% biotinylated tubulin). The long microtubules were perfused into the chamber from two sites with a 90° orientation towards each other. A stabilization mix containing BRB80, 0.5 mM GMPCPP and 10 μM ATTO-565-labelled tubulin was perfused into the chamber from both entry sites. After incubation for 5 min the stabilization mix was washed with 300 μl BRB80. The incorporation mix containing BRB80, 1 mM GTP and 20 μM ATTO-488-labelled tubulin was perfused from both sites and incubated for 7 min before washing with 300 μl BRB80 and imaging. The incorporations of green tubulin within a distance of 1 μm from the crossing site were taken into account as repair sites. 300 crossing sites from 3 independent experiments were analysed.

EB3 binding to photo damage sites in vitro

Red fluorescent microtubule seeds were randomly attached via neutravidin to cover glasses passivated with a mix of tri-ethoxy-silane-PEG-biotin and tri-ethoxy-silane-PEG. Seeds were elongated with red-fluorescent free tubulin (20% labelled, 16 μM) in presence of 100 nM EB3-GFP and standard buffer (see above) with 60 mM NaCl.

For experiments in the absence of free tubulin, microtubules were grown in a microfluidic chamber from red fluorescent seeds attached to micropatterns. Microtubules were grown with red fluorescent free tubulin (20% labelled, 20 μM) and protected from depolymerization with a cap of GMPCPP-tubulin (0.5 mM GMPCPP, 10 μM tubulin). Before photo damage, the solution was replaced by 100 nM EB3-GFP50 in standard buffer with 60 mM NaCl without free tubulin.

Statistics and reproducibility

All statistical analyses were performed using GraphPad Prism 6.0 or Microsoft Excel software. All results are presented in graphs are the mean ± SD. Each exact n value is indicated in the corresponding figure or figure legend. No statistical method was used to

Europe PMC Funders Author Manuscripts

predetermine sample size. No samples were excluded from the analyses. The investigators were not blinded to allocation during experiments and outcome assessment. A paired t-test was used in Fig. 7b. A Chi-square test was used in Fig, 5c. All experiments without quantification were independently performed at least three times and the representative data are shown.

Data availability

All data that support the conclusions are available from the authors on reasonable request.

Supplementary Material

Refer to Web version on PubMed Central for supplementary material.

Acknowledgements

We thank Guillaume Montagnac for sharing his unpublished data on tubulin photo-activation in cells; and Franck Perez and Christian Poüs for sharing their unpublished data on the microtubule rescue by Clip170. This work has been supported by an HFSP (RGY0088/2012), an ANR funding (ANR-12-BSV5-0014) and an ERC (Starting Grant 310472).

References

1. Mimori-Kiyosue Y. Shaping microtubules into diverse patterns: Molecular connections for setting up both ends. Cytoskeleton. 2011; 68:603–618. [PubMed: 22021191]
2. Hammond JW, et al. Posttranslational modifications of tubulin and the polarized transport of kinesin-1 in neurons. Mol Biol Cell. 2010; 21:572–83. [PubMed: 20032309]
3. Winans AM, Collins SR, Meyer T. Waves of actin and microtubule polymerization drive microtubule-based transport and neurite growth before single axon formation. Elife. 2016; 5:1–22.
4. Stiess M, et al. Axon extension occurs independently of centrosomal microtubule nucleation. Science. 2010; 327:704–7. [PubMed: 20056854]
5. Wadsworth P. Regional regulation of microtubule dynamics in polarized, motile cells. Cell Motil Cytoskeleton. 1999; 42:48–59. [PubMed: 9915584]
6. Waterman-Storer CM, Salmon ED. Actomyosin-based retrograde flow of microtubules in the lamella of migrating epithelial cells influences microtubule dynamic instability and turnover and is associated with microtubule breakage and treadmilling. J Cell Biol. 1997; 139:417–34. [PubMed: 9334345]
7. Gundersen GG, Bulinski JC. Selective stabilization of microtubules oriented toward the direction of cell migration. Cell. 1988; 85:5946–5950.
8. Akhtar N, Streuli CH. An integrin-ILK-microtubule network orients cell polarity and lumen formation in glandular epithelium. Nat Cell Biol. 2012; 15:17–27. [PubMed: 23263281]
9. Yi J, et al. Centrosome repositioning in T cells is biphasic and driven by microtubule end-on capture-shrinkage. J Cell Biol. 2013; 202:779–92. [PubMed: 23979719]
10. Sampath SC, et al. The chromosomal passenger complex is required for chromatin-induced microtubule stabilization and spindle assembly. Cell. 2004; 118:187–202. [PubMed: 15260989]
11. Grill SW, Go P, Hyman AA. Polarity controls forces governing asymmetric spindle positioning in the Caenorhabditis elegans embryo. Nature. 2001; 409:630–633. [PubMed: 11214323]
12. Labbe J, et al. PAR Proteins Regulate Microtubule Dynamics at the Cell Cortex in C . elegans The University of North Carolina at Chapel Hill. Current. 2003; 13:707–714.
13. Wen Y, et al. EB1 and APC bind to mDia to stabilize microtubules downstream of Rho and promote cell migration. Nat Cell Biol. 2004; 6:820–30. [PubMed: 15311282]
14. Etienne-manneville S, Hall A. Cdc42 regulates GSK-3 b and adenomatous polyposis coli to control cell polarity. Nature. 2003; 421:753–756. [PubMed: 12610628]

15. Fukata M, et al. Rac1 and Cdc42 capture microtubules through IQGAP1 and CLIP-170. Cell. 2002; 109:873–885. [PubMed: 12110184]
16. Dujardin DL, et al. A role for cytoplasmic dynein and LIS1 in directed cell movement. J Cell Biol. 2003; 163:1205–1211. [PubMed: 14691133]
17. Janson ME, de Dood ME, Dogterom M. Dynamic instability of microtubules is regulated by force. J Cell Biol. 2003; 161:1029–34. [PubMed: 12821641]
18. Komarova YA, Vorobjev IA, Borisy GG. Life cycle of MTs: persistent growth in the cell interior, asymmetric transition frequencies and effects of the cell boundary. J Cell Sci. 2002; 115:3527–39. [PubMed: 12154083]
19. Shelden E, Wadsworth P. Observation and quantification of individual microtubule behavior in vivo: Microtubule dynamics are cell-type specific. J Cell Biol. 1993; 120:935–945. [PubMed: 8432733]
20. Gardner MK, Zanic M, Howard J. Microtubule catastrophe and rescue. Curr Opin Cell Biol. 2013; 25:14–22. [PubMed: 23092753]
21. Walker RA, et al. Dynamic Instability of Individual Microtubules Analyzed by Video Light Microscopy: Rate Constants and Transition Frequencies. J Cell Biol. 1988; 107:1437–1448. [PubMed: 3170635]
22. Kowalski RJ, Williams RC. Microtubule-associated protein 2 alters the dynamic properties of microtubule assembly and disassembly. J Biol Chem. 1993; 268:9847–9855. [PubMed: 8486664]
23. Komarova YA, Akhmanova A, Kojima SI, Galjart N, Borisy GG. Cytoplasmic linker proteins promote microtubule rescue in vivo. J Cell Biol. 2002; 159:589–599. [PubMed: 12446741]
24. Al-Bassam J, et al. CLASP promotes microtubule rescue by recruiting tubulin dimers to the microtubule. Dev Cell. 2010; 19:245–258. [PubMed: 20708587]
25. Dimitrov A, et al. Detection of GTP-tubulin conformation in vivo reveals a role for GTP remnants in microtubule rescues. Science. 2008; 322:1353–6. [PubMed: 18927356]
26. Tropini C, Roth EA, Zanic M, Gardner MK, Howard J. Islands containing slowly hydrolyzable GTP analogs promote microtubule rescues. PLoS One. 2012; 7
27. Schaedel L, et al. Microtubules self-repair in response to mechanical stress. Nat Mater. 2015; doi: 10.1038/nmat4396
28. Billger MA, Bhatacharjee G, Williams RC. Dynamic instability of microtubules assembled from microtubule- associated protein-free tubulin: Neither variability of growth and shortening rates nor ‘rescue’ requires microtubule-associated proteins. Biochemistry. 1996; 35:13656–13663. [PubMed: 8885845]
29. Vitre B, et al. EB1 regulates microtubule dynamics and tubulin sheet closure in vitro. Nat Cell Biol. 2008; 10:415–21. [PubMed: 18364701]
30. Arnal I, Heichette C, Diamantopoulos GS, Chrétien D. Clip-170/Tubulin-Curved Oligomers Coassemble at Microtubule Ends and Promote Rescues. Current. 2004; 14:2086–2095.
31. Wightman R, Turner SR. Severing at sites of microtubule crossover contributes to microtubule alignment in cortical arrays. Plant J. 2007; 52:742–751. [PubMed: 17877711]
32. Zhang Q, Fishel E, Bertroche T, Dixit R. Microtubule Severing at Crossover Sites by Katanin Generates Ordered Cortical Microtubule Arrays in Arabidopsis. Curr Biol. 2013; 23:2191–2195. [PubMed: 24206847]
33. Davis LJ, Odde DJ, Block SM, Gross SP. The Importance of Lattice Defects in Katanin-Mediated Microtubule Severing in Vitro. Biophys J. 2002; 82:2916–2927. [PubMed: 12023214]
34. Díaz-Valencia JD, et al. Drosophila katanin-60 depolymerizes and severs at microtubule defects. Biophys J. 2011; 100:2440–9. [PubMed: 21575578]
35. Walker RA, Inou S, Salmon ED. Asymmetric Behavior of Severed Microtubule Ends After Ultraviolet-Microbeam Irradiation of Individual Microtubules In Vitro. Cell. 1989; 108:931–937.
36. VanBuren V, Cassimeris L, Odde DJ. Mechanochemical model of microtubule structure and self-assembly kinetics. Biophys J. 2005; 89:2911–2926. [PubMed: 15951387]
37. Portran D, Gaillard J, Vantard M, Théry M. Quantification of MAP and molecular motor activities on geometrically controlled microtubule networks. Cytoskeleton (Hoboken). 2013; 70:12–23. [PubMed: 23027541]

38. Alushin GM, et al. High-Resolution Microtubule Structures Reveal the Structural Transitions in αβ-Tubulin upon GTP Hydrolysis. Cell. 2014; 157:1117–1129. [PubMed: 24855948]
39. Bowne-Anderson H, Zanic M, Kauer M, Howard J. Microtubule dynamic instability: A new model with coupled GTP hydrolysis and multistep catastrophe. BioEssays. 2013; 35:452–461. [PubMed: 23532586]
40. Zhang D, et al. Drosophila katanin is a microtubule depolymerase that regulates cortical-microtubule plus-end interactions and cell migration. Nat Cell Biol. 2011; 13:361–70. [PubMed: 21378981]
41. Charafeddine RA, et al. Fidgetin-Like 2: A Microtubule-Based Regulator of Wound Healing. J Invest Dermatol. 2015; 135:2309–18. [PubMed: 25756798]
42. Ward A, et al. Solid friction between soft filaments. Nat Mater. 2015; 14:583–588. [PubMed: 25730393]
43. Doodhi H, Katrukha EA, Kapitein LC, Akhmanova A. Mechanical and Geometrical Constraints Control Kinesin-Based Microtubule Guidance. Curr Biol. 2014; :1–7. DOI: 10.1016/j.cub.2014.01.005
44. Ahmadzadeh H, Smith DH, Shenoy VB. Mechanical Effects of Dynamic Binding between Tau Proteins on Microtubules during Axonal Injury. Biophys J. 2015; 109:2328–2337. [PubMed: 26636944]
45. Bechstedt S, Brouhard GJ. Doublecortin recognizes the 13-protofilament microtubule cooperatively and tracks microtubule ends. Dev Cell. 2012; 23:181–92. [PubMed: 22727374]
46. Shelanski ML. Chemistry of the filaments and tubules of brain. J Histochem Cytochem. 1973; 21:529–39. [PubMed: 4358987]
47. Malekzadeh-Hemmat K, Gendry P, Launay JF. Rat pancreas kinesin: identification and potential binding to microtubules. Cell Mol Biol (Noisy-le-grand). 1993; 39:279–85. [PubMed: 8334381]
48. Hyman A, et al. Preparation of modified tubulins. Methods Enzymol. 1991; 196:478–85. [PubMed: 2034137]
49. Portran D, et al. MAP65/Ase1 promote microtubule flexibility. Mol Biol Cell. 2013; 24:1964–73. [PubMed: 23615441]
50. Komarova YA, et al. Mammalian end binding proteins control persistent microtubule growth. J Cell Biol. 2009; 184:691–706. [PubMed: 19255245]

Europe PMC Funders Author Manuscripts

Europe PMC Funders Author Manuscripts

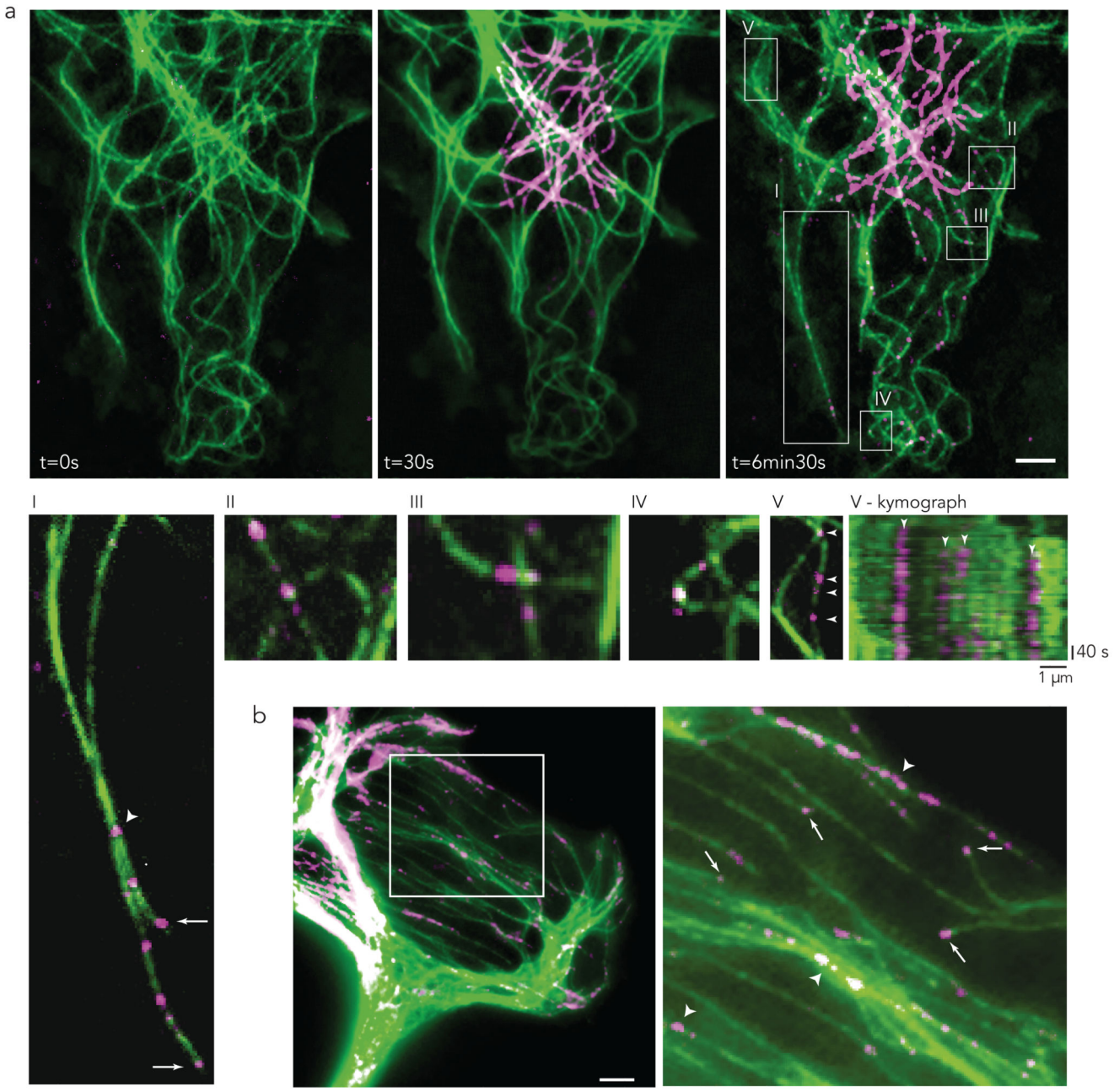

Figure 1. Microtubule self-repair in living cells.

(a) PTK2 cell expressing mEos2 pre- and post-conversion. Converted free tubulin dimers (magenta) diffused through the cytoplasm. Signal of converted dimers (magenta) was observed at the growing tips as well as in spot-like structures along the length of pre-existing microtubules (green).

(I-V) Enlarged regions of a.

(I) Bundled microtubules with photo-converted tubulin spots within the bundle (arrowhead) and at the growing tip (arrow).

(II-III) Incorporation of converted dimers (magenta) in pre-existing microtubule (green) at microtubule crossing sites.
(IV) Incorporation of converted dimers (magenta) in pre-existing microtubule (green) at bent sites.
(V) Incorporation along pre-existing microtubule (arrowhead) with corresponding kymograph. Bottom white arrowhead in (V) is represented by the first left arrowhead of the kymograph in (V-kymograph).
(b) After photo-conversion magenta-tubulin signal was observed at growing microtubule tips (arrow). True incorporation was not distinguishable from growing tips within bundled microtubules (arrowhead).
Arrows are growing microtubule tips after photo-conversion; arrowheads are sites of incorporation of converted tubulin dimers (magenta) in pre-existing microtubule. Images are representative of 5 independent experiments. Scale bar 5 μm.

Europe PMC Funders Author Manuscripts

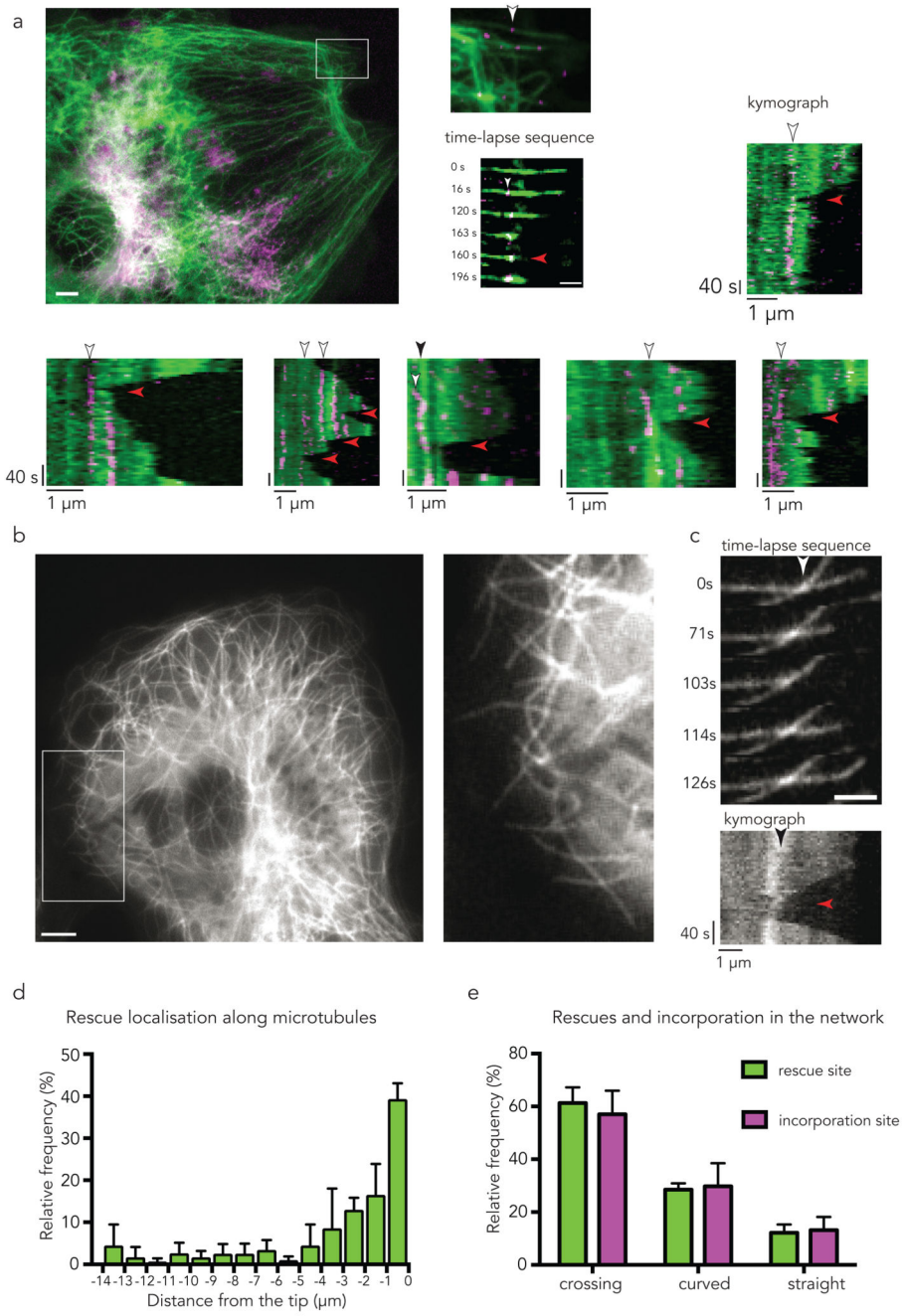

Figure 2. Self-repair sites are rescue sites in living cells.

(a) Photo-converted tubulin dimers (magenta) in pre-existing microtubule (green). The white arrow head in the inset point at a repair site along a single microtubule. Scale bar 5 µm. The time-lapse sequence shows the occurrence of a rescue event (red arrow head) at the site of incorporation with corresponding kymograph (right panels). Scale bar 2 µm. Kymographs at the bottom show additional examples of repair sites (white arrow heads) associated with rescue events (red arrow heads). Kymograph in the third panel shows an incorporation

(white arrow head) and rescue event (red arrow head) at a microtubule crossing site (black arrow head). Images are representative of 5 independent experiments.

(b) The localization of rescue events were analysed within the cell margin of PTK2 cells stably expressing GFP-tubulin. Enlarged region (white rectangle) of a representative analysed area. Scale bar 5 μm.

(c) Representative time sequence of a rescue event at a microtubule crossing site (white arrowhead) with corresponding kymograph. Black arrow indicates the crossing site within the kymograph, the red arrow points at the rescue event. Images in 2 b,c are representative of 5 independent experiments. Scale bar 2 μm.

(d) Histogram of the distance of rescue events with respect to the growing tip (set to zero) in PTK2 GFP-tubulin cells. Data represent mean +/- s.d, n= 148 rescue events from 4 cells.

(e) Correlation of the site of rescue with the site of incorporation. Relative frequency of the localization of the rescue event with respect to crossing sites, curved sites and straight microtubules. Relative frequency of the localization of the incorporation with respect to crossing sites, curved sites and straight microtubules. Incorporation was analysed in fixed cells 2 min after photo-conversion. Data represent mean +/- s.d, n= 79 rescue events from 4 cells, and n= 113 incorporation events from 4 cells.

Europe PMC Funders Author Manuscripts

Europe PMC Funders Author Manuscripts

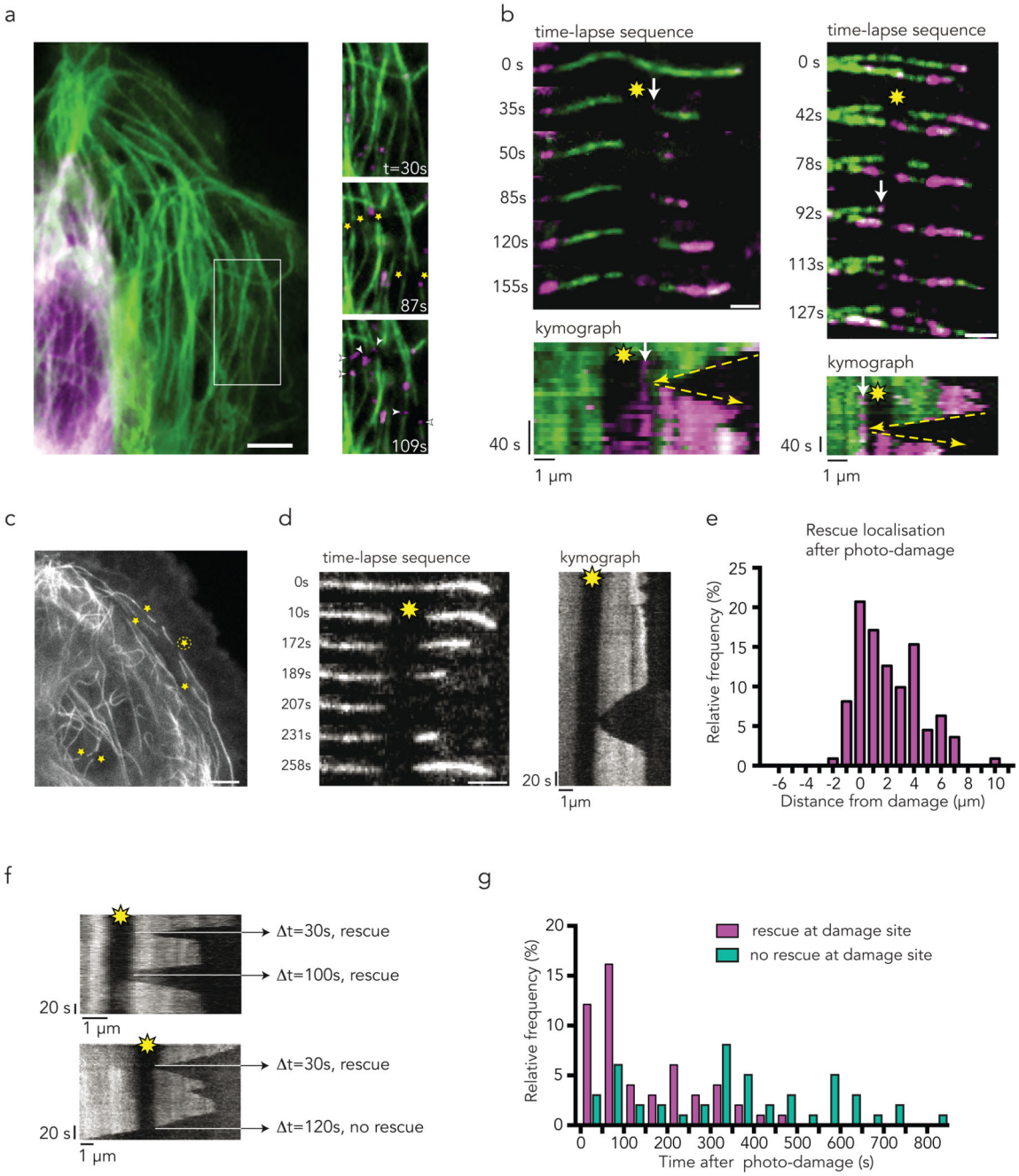

Figure 3. Photo-damaged sites are repair and rescue sites in living cells.

Yellow star indicates photo-damage sites; white arrow indicates site of incorporation of photo-converted tubulin dimers (magenta). Yellow arrow is tracking the depolymerisation, rescue, and growth event.

(a) Laser induced photo-damage sites (star) get repaired (arrowhead) by converted tubulin dimers (magenta) over time.

(b) Time-lapse sequence with corresponding kymographs of microtubules after laser induced photo-damage (yellow star). Incorporation (arrow) of converted tubulin dimers (magenta)

occurs at the photo-damage sites and act as rescue sites. Note within the kymographs that rescue occurs at the exact position of repair site, highlighted by yellow arrows. Scale bar 2 μm.

(c) Representative sites of laser induced photo-damage within the cell margin and near the nucleus (yellow stars) of PTK2 GFP-tubulin cells. Time sequence and kymograph of the rescue event of the microtubule labelled with an encircled star is shown in d. Scale bar 5 μm.

(d) Representative time-lapse sequence and corresponding kymograph of analysed microtubule after photo-damage (yellow star). Microtubule rescues at the photo-damage site. Images are representative of 5 independent experiments. Scale bar 2 μm.

(e) Histogram of the localization of the 111 rescue events with respect to the 51 photo-damage site in 20 PTK2 GFP-tubulin cells. All rescues occurring along the microtubule tip were taken into account. Center of the photo-damage site is x = zero; average size of photo-damage was 1.2 μm. 50 % of the rescues occurred within the damage site. Only one rescue event was observed shortly after the damage site. The other 50% of rescues were observed along the microtubule closer to the tip, where the frequency of rescue is reported to be high.

(f) Multiple rescues at a photo-damage site (yellow star) were observed occasionally. Microtubule depolymerized eventually over the photo-damage site after rescue events (bottom image).

(g) Histogram of the time between the induction of photo-damage (t= 0 s) and observation of the rescue or depolymerization event in 10 cells showing 52 rescues at damaged site and 47 absence of rescue at damaged sites. Rescue events are most frequent within 250 s after photo-damage. No rescue was observed after 550 s.

Europe PMC Funders Author Manuscripts

Europe PMC Funders Author Manuscripts

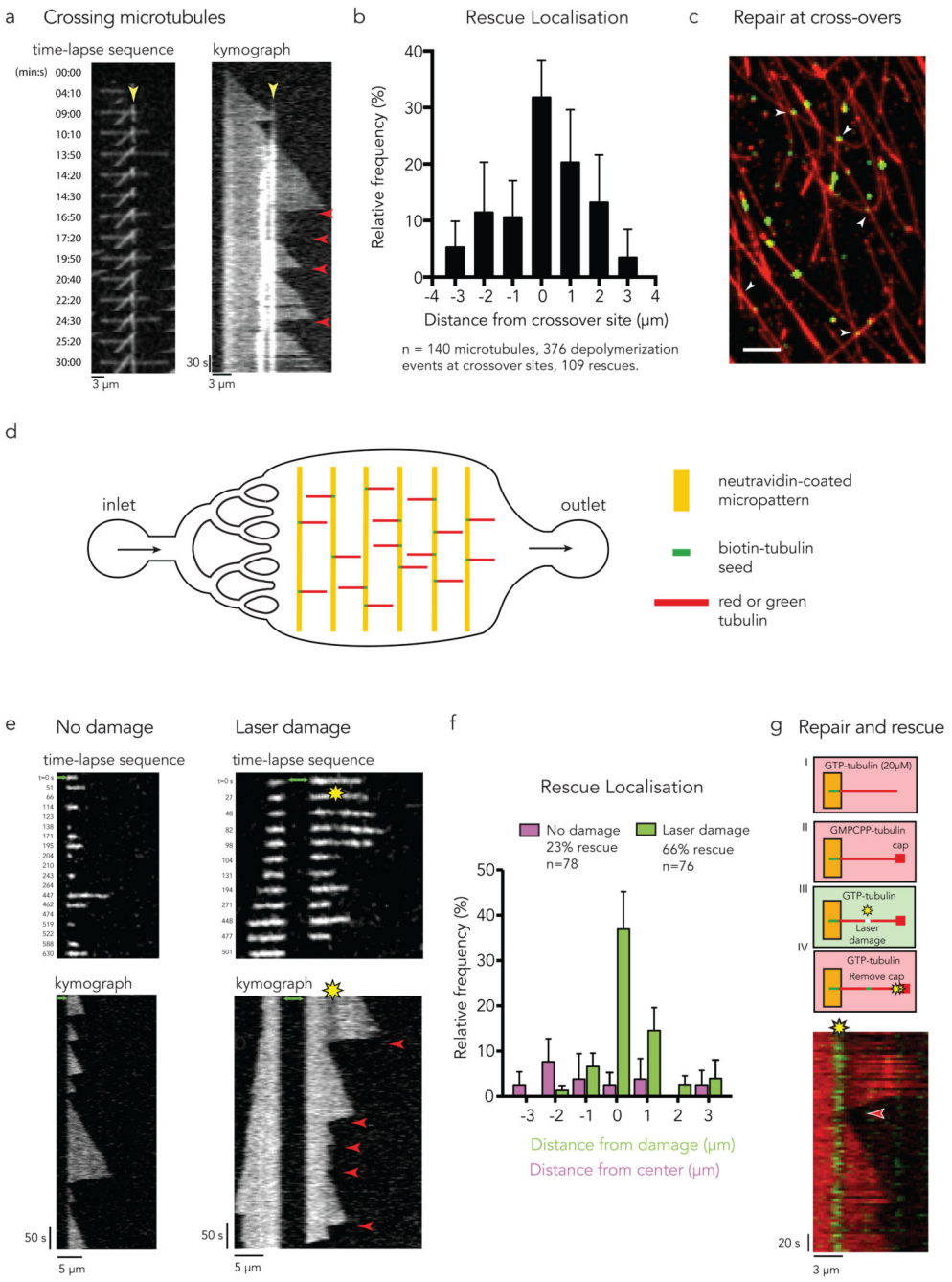

Figure 4. Microtubule self-repair induces rescue events in vitro.

(a) Rescue at crossing microtubules. Time-lapse sequence of 3 microtubules crossing each other. The kymograph highlights the crossing sites (yellow arrow-head pointing at the bright white vertical lines) and the occurrence of multiple rescue events at this site (red arrow-heads).

(b) The graph shows the frequency of rescue events for crossing microtubules as a function of distance from the crossing site. Data represent mean +/- s.d from n=8 independent experiments.

(c) Repair at crossing microtubules. Observation of the incorporation of green tubulin dimers along red microtubules. White arrow-heads point at crossing sites where accumulation of green tubulin was detected. Image is representative of 3 independent experiments. Scale bar 5 μm.

(d) Illustration of the microfluidic device. Short biotinylated microtubule seeds were fixed on neutravidin coated micropatterns and elongated using red or green free tubulin. To exchange or remove the solution of free tubulin, a flow was induced parallel to the microtubules.

(e) Photo damage sites can induce rescue. The image sequences and kymographs show microtubule dynamics with (right) and without (left) laser-induced damage. The green arrows indicate the seed. Red arrow-heads indicate rescue events.

(f) The graph shows the frequency of rescue events for photo damaged microtubules as a function of distance from the center of the damage (green bars) and for microtubules without damage as a distance from the center of the observed microtubule (magenta bars). Data represent mean values +/- s.d from n= 4 independent experiments.

(g) Tubulin incorporation at photodamaged sites is associated with rescue. Green microtubule seeds were elongated with red free tubulin (step I). A GMPCPP cap was grown at the microtubule tip to avoid spontaneous depolymerization (step II). Photo damage was induced in the presence of green tubulin (step III). Depolymerization was initiated by removing the GMPCPP cap with a laser pulse at high intensity (step IV). The kymograph shows rescue (red arrow-head) at the damaged site where green tubulin was incorporated. Image is representative of 4 independent experiments.

Europe PMC Funders Author Manuscripts

Europe PMC Funders Author Manuscripts

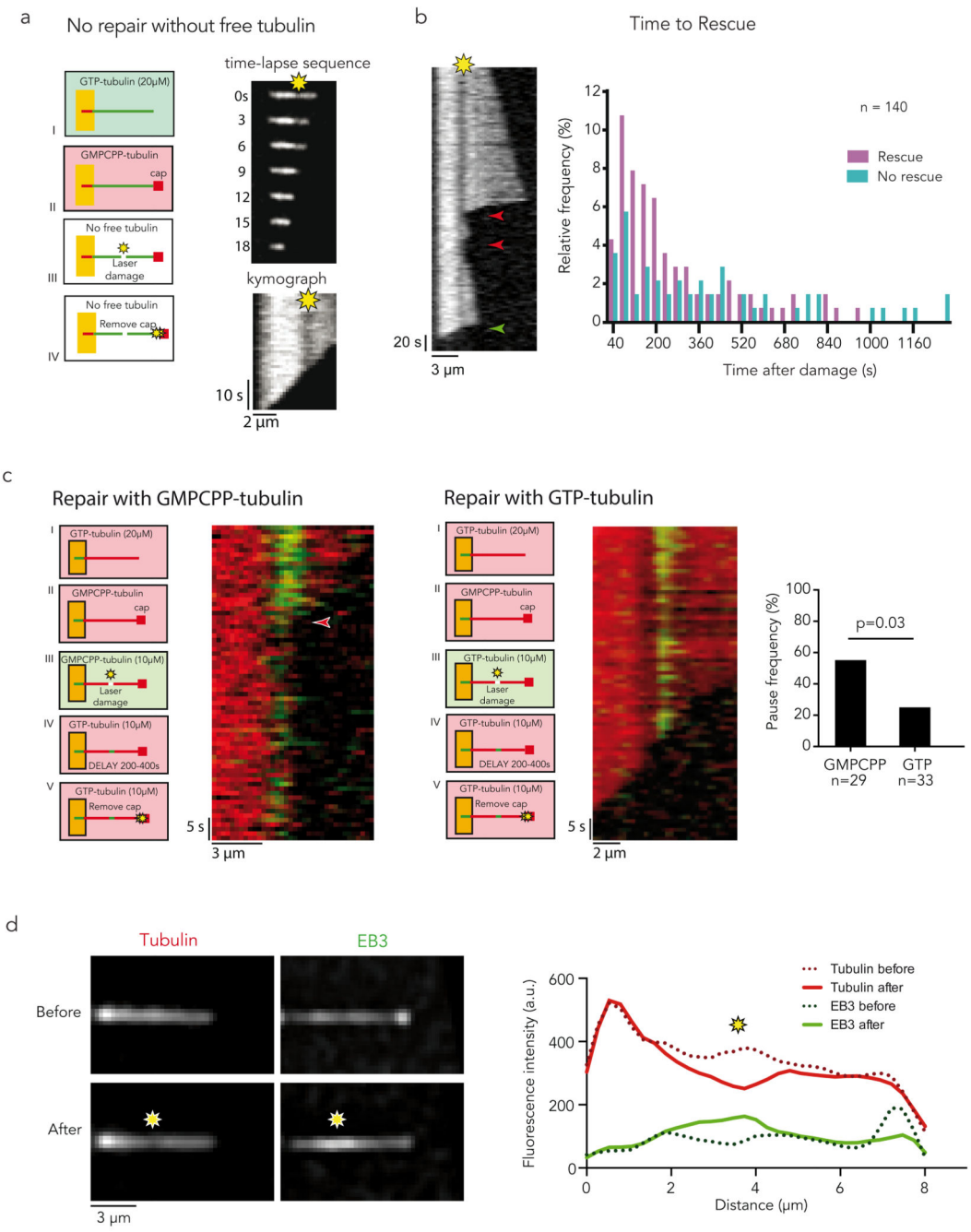

Figure 5. Incorporation and hydrolysis of free tubulin.

(a) Damage without repair. Red microtubule seeds were elongated with green free tubulin (step I). A GMPCPP cap was grown at the microtubule tip to avoid spontaneous depolymerization (step II). Photo damage was induced in the absence of free tubulin (step III). Depolymerization was initiated by removing the GMPCPP cap with a laser pulse at high intensity (step IV). The time-lapse sequence and kymograph show no rescue nor pause at the damaged, and non-repaired, site. See quantification in supplementary figure 4.

Europe PMC Funders Author Manuscripts

(b) Rescue Lifetime. Kymograph shows multiple rescues (red arrow-heads) at a photo-damage site (yellow star) eventually followed by microtubule depolymerisation (green arrow-head). The graph represents the time between inducing the damage and observation of the rescue or depolymerisation event. Rescue events become less frequent as the time after damage increases. No rescue could be observed 17 minutes after inducing the damage.
(c) Hydrolysis of incorporated tubulins. Red microtubules were laser damaged and repaired with non-hydrolyzable (GMPCPP, left panels) or hydrolysable (GTP, right panels) tubulin. After an additional delay of 3 to 6 minutes the cap was removed in the presence of sub-critical concentration of free tubulin. The graph shows the frequency of pauses (highlighted in the left panel with a red arrow-head) in both cases. Non-hydrolysable tubulins increased the lifetime of repair and rescue sites. A Chi-square test was used to compare pause frequencies for GTP and GMPCPP. n represents the number of microtubules that were allowed to repair in the presence of GTP and GMPCPP, respectively.
(d) EB3 recruitment at repair sites. Red microtubules were photodamaged in the presence of red-fluorescent free tubulin dimers and EB3-GFP. Images show microtubule fluorescence in the red (left) and green (right) channels, before (top) and after (bottom) the laser-induced damage. The graph shows fluorescent linescans along this microtubule before and after the damage. The yellow star represents the damaged site. More examples are shown in Supplementary Figure 5 as well as absence of EB3 recruitment in the absence of free tubulin. Images are representative of 5 independent experiments.

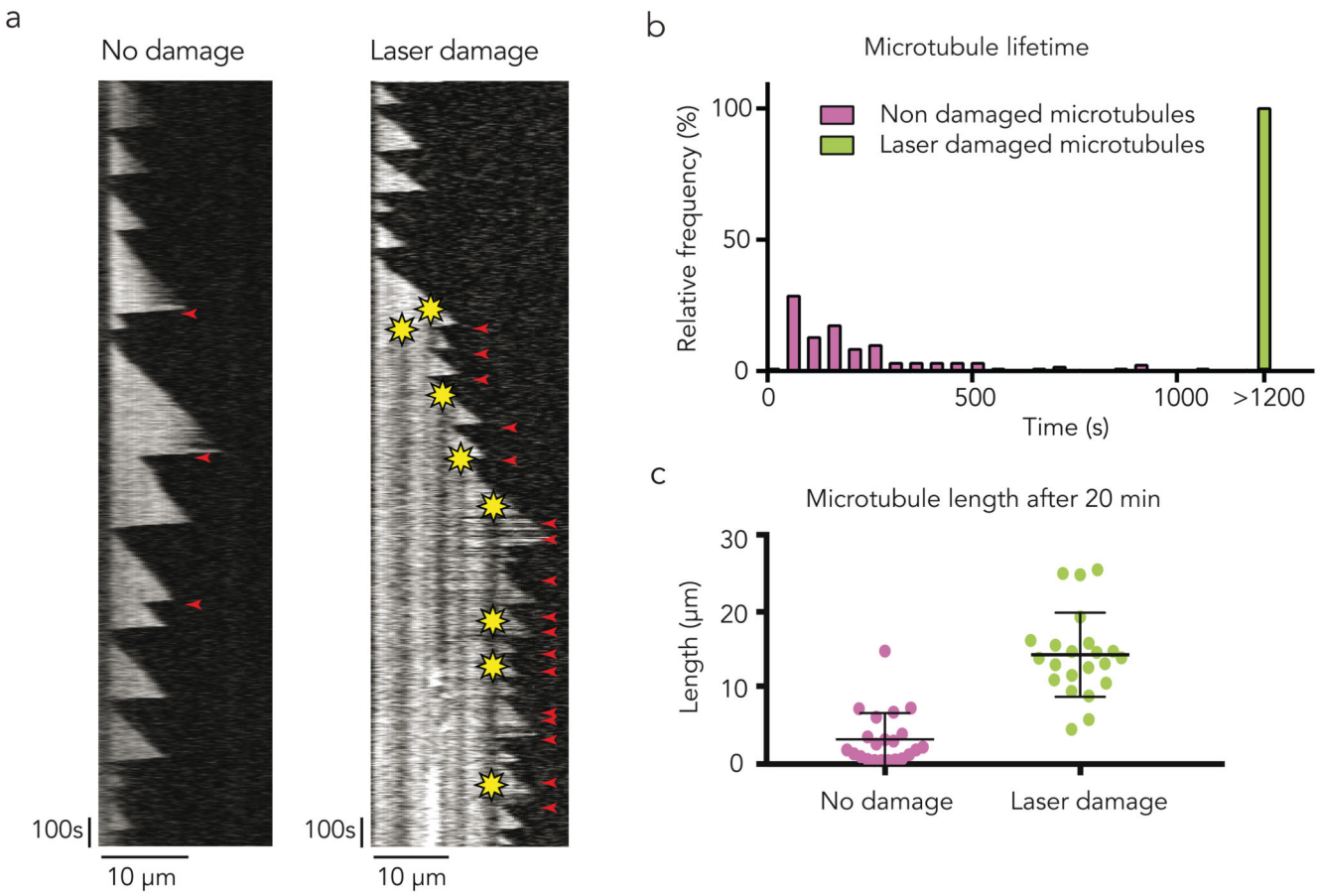

Figure 6. Self-repair biases microtubule dynamic instability in vitro.

(a) The kymograph on the left shows a typical non-damaged microtubule with infrequent rescue events. On the right, the microtubule was damaged several times close to the tip as soon as it grew out long enough. Though catastrophe events were frequent, this microtubule was protected from complete depolymerisation by the photo damage. Yellow star indicates the photo-damage site. Red arrowhead indicates rescue events.

(b) Damages increase microtubule lifetime. The graph shows the distribution of 28 laser damaged (green) and 133 non-damaged (magenta) microtubule lifetime. Damaged microtubule lifetime was found to be considerably longer than the lifetime of non-damaged microtubules.

(c) Damages increase microtubule length. The graph shows the length of laser damaged (green) and non-damaged (magenta) microtubule after 20 minutes. Error bars show mean +/- s.d. for n = 22 microtubules per condition, pooled from 4 independent experiments.

Europe PMC Funders Author Manuscripts

Europe PMC Funders Author Manuscripts

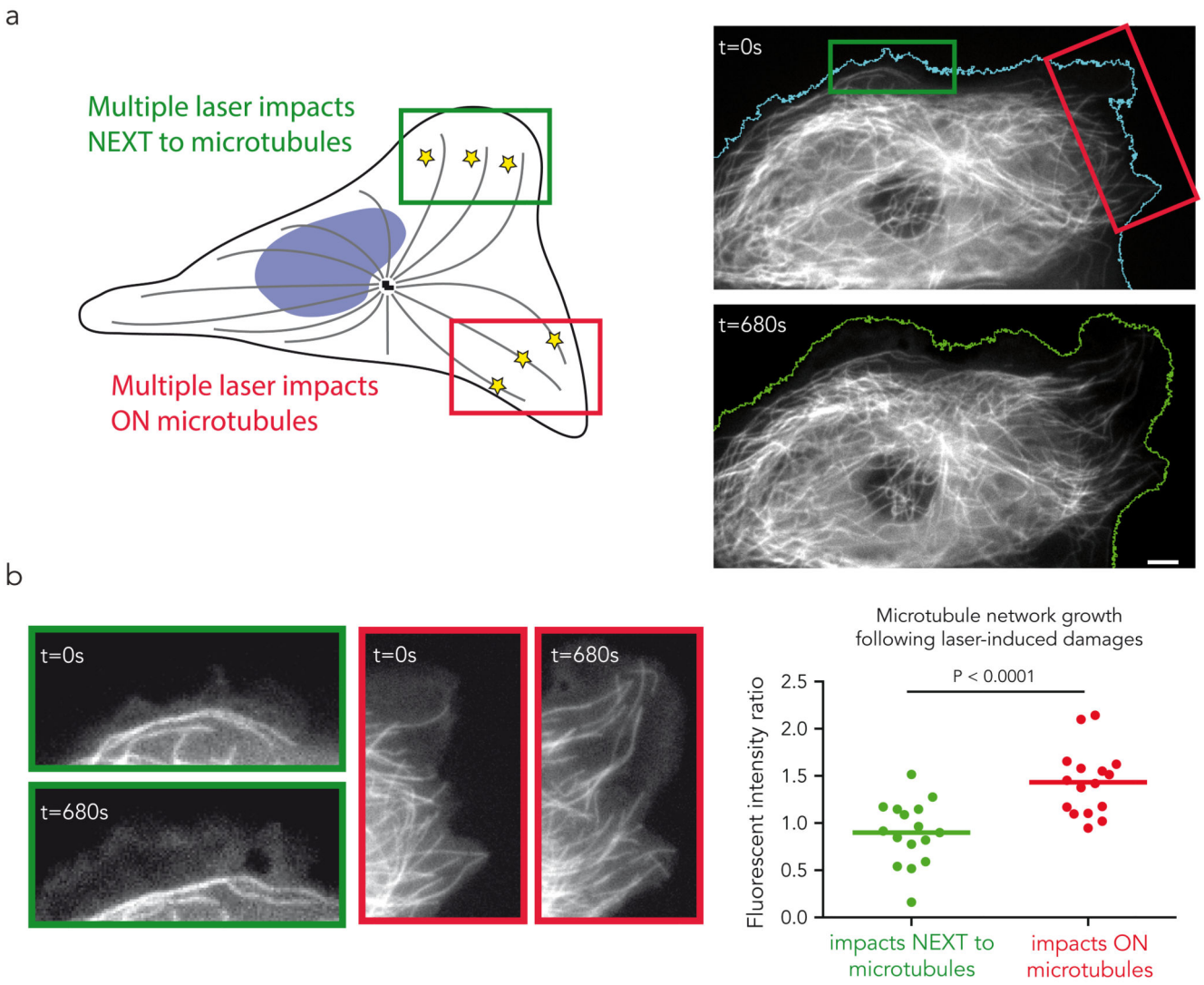

Figure 7. Self-repair biases microtubule dynamic instability in vivo.

(a) Repeated microtubule shooting “on” and “off-target”. Laser induced photo-damage were targeted either on the microtubules, in the red region, or next to the microtubules, in the green region. The images show the cell before (top) and after (bottom) the shooting. Comparison of the left and right cell margin pre- and post-photo-damage. Scale bar is 5 μm. **(b)** Preferential microtubule network growth in damaged regions. Images show the microtubule network in the “on-target” (red) and “off-target” (green) regions before (t=0s) and after (t=680s) the shooting. The graph shows the after/before ratio of the mean microtubule fluorescence intensity in each region. Lines represent mean values from n=16 cells from 4 independent experiments. P value was generated by a wilcoxon paired test. The total microtubule length increased in the regions where the laser impacts were targeted on the microtubules. Scale bar is 2 μm.

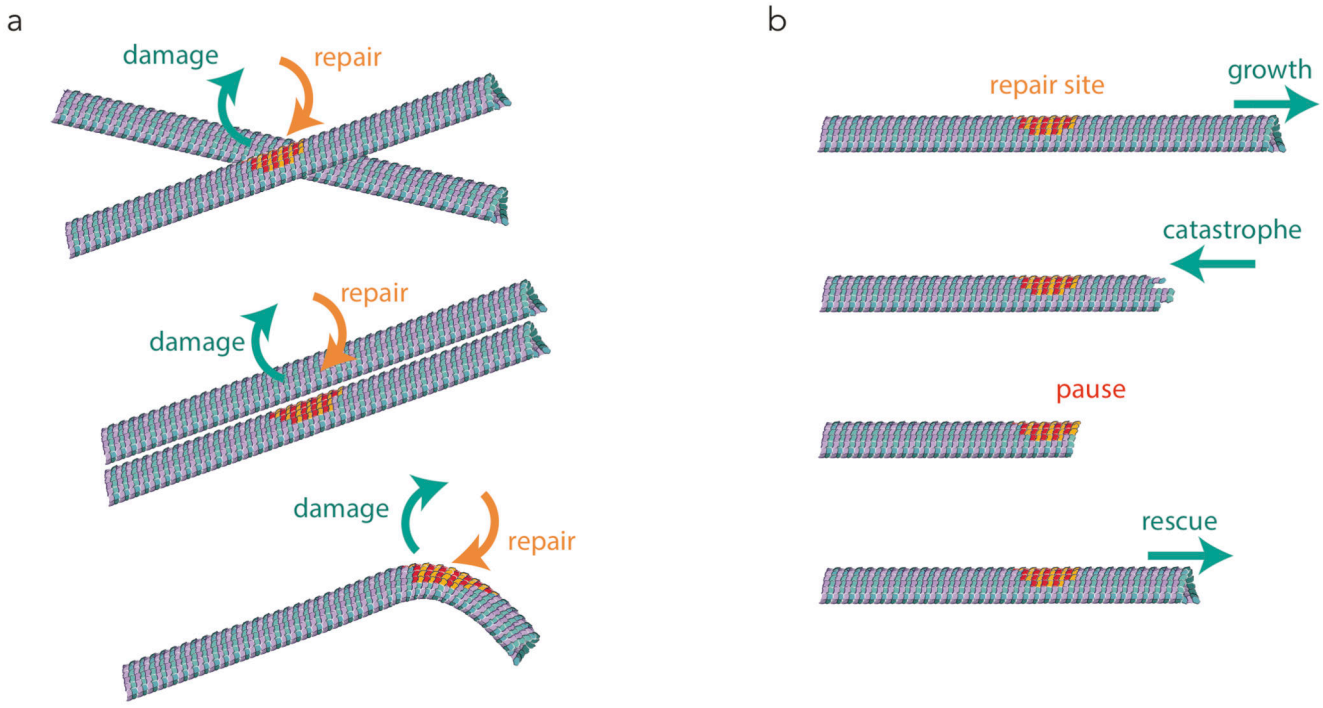

Figure 8. Microtubule self-repair and rescue.

(a) Microtubule self-repair. The schemes show the preferential microtubules' conformation in which free tubulin incorporation (orange-red) was observed along pre-existing microtubules (green-blue) in living cells.

(b) Microtubule rescue at self-repair sites. The schemes show the interruption of microtubule depolymerisation at the repaired site (shown with orange-red dimers) and the induction of microtubule regrowth.

Europe PMC Funders Author Manuscripts